Classification of Local Climate Zones Based on Multiple Earth Observation Data

Benjamin Bechtel and Christian Daneke

***Abstract*—Considerable progress was recently made in the determination of urban morphologies or structural types from different Earth observation (EO) datasets. A relevant field of application for such methods is urban climatology, since specific urban morphologies produce distinct microclimates. However, application and comparability are so far limited by the variety of typologies used for the description of urban surfaces in EO. In this study Local Climate Zones (LCZ), a system of thermally homogenous urban structures introduced by Stewart and Oke, was used in a pixel-based classification approach. Further, different EO datasets (including satellite multitemporal thermal and multispectral data as well as a normalized digital surface model (NDSM) from airborne Interferometric Synthetic Aperture Radar) and different classifiers (including Support Vector Machines, Neural Networks and Random Forest) were evaluated for their performance in a common framework. Especially the multitemporal thermal and spectral features yielded high potential for the discrimination of LCZ, but morphological profiles from the NDSM also performed well. Further, sets of 10–100 features were selected with the Minimum Redundancy Maximal Relevance approach from multiple EO data. Overall classification accuracies of up to 97.4% and 95.3% were obtained with a Neural Network and a Random Forest classifier respectively. This provides some evidence that LCZ can be derived from multiple EO data. Hence, we propose the typology and the method for the application of automated extraction of urban structures in urban climatology. Further the chosen multiple EO data and classifiers seemed to yield considerable potential for an automated classification of LCZ.**

***Index Terms*—IFSAR, image classification, Landsat, local climate zones, multi-temporal, multiple earth observation.**

ABBREVIATIONS AND NOTATIONS:

ACP	Annual Cycle Parameters
DAFE	Discriminant Analysis Feature Extraction
DBFE	Decision Boundary Feature Extraction
DSM	Digital Surface Model
DTM	Digital Terrain Model
EO	Earth Observation
ETM+	Enhanced Thematic Mapper Plus
FFT	Fast Fourier Transform
I	Mutual Information
IFSAR	Interferometric Synthetic Aperture Radar
LCZ	Local Climate Zones
LIDAR	Light Detection and Ranging
MAST	Mean Annual Surface Temperature
MID	Mutual Information Difference
MIQ	Mutual Information Quotient
ML	Maximum Likelihood
MRMR	Minimum Redundancy Maximal Relevance
MS	Multispectral
NB	Naive Bayes
NDSM	Normalized Digital Surface Model
NDVI	Normalized Differenced Vegetation Index
NN	Neural Network
NWFE	Nonparametric Weighted Feature Extraction
OA	Overall Accuracy
PA	Producer Accuracy
RF	Random Forest
SAGA	System for Automated Geoscientific Analyses
SVM	Support Vector Machines
TIR	Thermal Infrared
TM	Thematic Mapper
UA	User Accuracy
UHI	Urban Heat Island
VHR	Very High Resolution
Weka	Waikato Environment for Knowledge Analysis
YAST	Yearly Amplitude of Surface Temperature
κ	Kappa-estimate

Manuscript received October 27, 2011; revised January 09, 2012; accepted February 08, 2012. Date of publication April 18, 2012; date of current version July 20, 2012.

B. Bechtel is with the University of Hamburg, Geosciences, Hamburg 20146, Germany (corresponding author, e-mail: benjamin.bechtel@uni-hamburg.de).

C. Daneke is with the University of Hamburg, Geosciences, Hamburg 20146, Germany, (e-mail: christian.daneke@uni-hamburg.de).

Color versions of one or more of the figures in this paper are available online at http://ieeexplore.ieee.org.

Digital Object Identifier 10.1109/JSTARS.2012.2189873

I. INTRODUCTION

IT is well-known that specific urban structures and morphologies produce distinct microclimates. The urban heat island (UHI) [1], as the most prominent example, is not uni-

formly distributed but clearly differentiated within the urban fabric [2]–[4] and was therefore also denoted an urban heat archipelago [5]. Earth Observation (EO) contributes to the characterization of urban climate in several ways, which were recently reviewed in [6] and include direct flux measurements [7] and biophysical parameters for the characterization of urban thermal landscapes. Urban climatology could further profit from an automated classification tool for urban morphologies with respect to their thermal effects.

During the last decade, the automated classification of urban structures based on improved classifiers and different datasets made considerable progress. Especially, SAR-data [8]–[10], hyperspectral data [10]–[14], hyperspectral and thermal [15], multitemporal thermal [16], and very high resolution (VHR) optical [17], [18] data were applied on the extraction of urban surfaces and structures. Besides, combined multisensor approaches were tested [9], [19] .

However, the application of these methods is severely limited by the diversity of typologies used for the distinction of the occurring urban morphologies. While some merely distinguish between *water*, *vegetation* and *build*, other studies used further land cover classes (*houses*, *streets*, *trees*, *soil*) [18] up to highly detailed typologies of surface materials (e.g., *bitumen*, *concrete*, *asphalt*, *tar*) [13]. Classification systems for urban structures were referred to as urban structural types, urban morphologies, structures or zones. These classes were mostly defined qualitatively (if at all), partly mixing concepts of function and form. This variation results in limited transferability and poor comparability of the results.

Similarly, in urban climatology various schemes of urban sites exist – often rather resulting from a pragmatic use of the available data infrastructures (e.g., biotope mappings) then an integrated concept. Oke [20] demanded a common set of classes and descriptions to improve scientific communication and overcome the 'urban-rural dichotomy' [21]. Hence, a common typology of urban landscapes or morphologic classes could not only serve as a standard for both urban climatology and urban remote sensing, but also as an interface between the disciplines and was required for the routine application of urban structures classified from EO data in urban climatology.

A typology with the particular potential to become such a standard in urban climatology was recently introduced by Stewart & Oke [22]. Their classification system of local (thermal) climate zones (LCZ) is based on various former typologies and explicitly defines urban landscapes according to their thermal properties. The typology aims to be objective (incorporating measurable and testable features relevant to surface thermal climate), inclusive (sufficiently generic in its representation of local landscapes to not inherit regional or cultural biases) and standardized. The individual classes aim to have 'relatively' homogenous air temperature within the canopy layer. They are defined by fact sheets with both qualitative and quantitative properties including several features that can be derived from EO data, like albedo [23], built fraction [24] and aerodynamic roughness [25]. This fosters applicability of the LCZ scheme as an interface between earth observation and urban climatology.

Essentially, two approaches – object-based and pixel-based – can be followed to extract urban morphological structures. As stated before, up-to-date datasets allow classification and monitoring of surface materials. Since each specific urban class comprises various surface materials, the classified data needs to be transferred to a lower level of detail (e.g., from single houses to building blocks). Object-based methods allow the aggregation of a first image segmentation into more meaningful urban structures or morphologies. Wurm and colleagues utilized VHR optical satellite imagery and a digital surface model derived by airborne LIDAR (Light detection and ranging) to retrieve 'urban structural types' in an object-oriented multilevel fuzzy classification scheme [17]. However, the object-oriented approach remains challenging, taking into consideration that urban structures are amongst the most complex ones on the Earths' surface. As a consequence, tremendous context knowledge is required turning the analysis into a demanding task for (knowledge-based) computer vision.

Since the targeted product – (microclimatic homogenous) urban structures – does not require the high level of detail, the less sophisticated pixel-based approach may as well be considered. This approach abandons segmentation but directly classifies the pixels (at a lower level of detail). Hence, the information in the spatial domain is not exploited and no coded context knowledge is needed.

In this study, an extended pixel-based approach was chosen using mathematical morphology and Fourier techniques on a higher resolution normalized digital surface model (NDSM) in order to create a 'joint spectral/spatial classifier' [11] or merely incorporate geometric and texture information within the classification process. To foster the automated classification of LCZ, the chosen EO features should best be related to specific urban climatologic processes. For further discussion of this relation and the conceptual idea of the classification approach see [26].

This study focuses on the following questions. 1. Can LCZ be automatically classified from multiple source satellite and airborne Earth observation data for monitoring of the built environment? 2. Can the classification scheme be adapted to European urban Morphologies? 3. Which of the tested datasets have the highest potential for an automated classification of LCZ? And 4. which algorithms are most suitable?

The paper is organized as follows. In Section II the land use typology and data and the different features sets are introduced. Further, the minimum redundancy maximum relevance feature selection and the classifiers are briefly explained. Classification results using single and multiple feature sets are presented in Section III and discussed in Section IV. Conclusions and an outlook are given in Section V.

II. Data and Methods

A. Training Data and Local Climate Zones

The thermal local-scale landscape classification system used in this study was introduced by Stewart and Oke [22]. It was proposed to overcome the dichotomous classification of 'rural' versus 'urban' in urban climatology and deliver a better categorization for measurement sites. It has a high potential to become a standard in urban climatology due to its clear criteria

TABLE I
TYPOLOGY OF URBAN LANDSCAPES; TRAINING AND TESTING DATA

class	LCZ (Stewart & Oke)	Num Pixels	test	train
blocks	Blocks	161	44	117
field	Cropped/Bare Fields	1663	396	1267
forest	Forest	2677	682	1995
gardens	-	95	35	60
industr	Industrial/ Extensive Lowrise	626	163	463
modcore	Modern Core	55	14	41
park	Grasslands	141	34	107
port	Extensive Lowrise	1113	305	808
rail	-	78	16	62
reghous	Regular Housing	357	80	277
terrace	Compact Housing	119	31	88
urbcore	Old Core	165	41	124
urbdens	Compact Housing	634	165	469
water	-	417	112	305

and the incorporation of previous systems such as [27]. The differentiation of local landscapes strictly followed their microclimatic characteristics. The landscapes were first divided by their surface disturbance into city, agricultural, natural and mixed [22]. Each of these series was further divided according to microscale (10s–100s of meters) surface properties which affect the canopy-layer thermal climate. Hence, the classes were defined by six properties – the sky view factor, the fraction of impervious materials, the Davenport roughness class [28], the surface thermal admittance and the mean annual anthropogenic heat flux.

Although the LCZ typology is supposed to be generic and not include any cultural bias, a certain predisposition towards Northern American morphologies can be assessed. Since the scheme is still in progress and both slightly different classes [29] and properties [30] were presented by the authors, the classification system used for this study maintains maximal compatibility with the first LCZ scheme despite its slight differentiation (cf. Table I).

In our study, the urban classes were subdivided into the following categories. Old urban Core (*urbcore*) representing the historic inner city with large representative buildings such as the town hall. Buildings in general are massive and uniformly high with spires reaching out of the skyline (Fig. 1(a)). Due to the higher variety of compact morphologies in Europe, the LCZ 'Compact Housing' was split into two classes. Urban Dense (*urbdens*) refers to perimeter block buildings as usually built in the Wilhelminian time. The morphology shows large buildings of a uniform height, built in blocks with courtyards in the center (Fig. 1(b)). Terraced Housing (*terrace*) describes a regular pattern of buildings aligned in rows. The spacing in-between and the height are mostly uniform, thus lower than the previous classes (Fig. 1(c)). The difference between the two is clearly recognizable in the pictograms. *Blocks* are high-rise buildings showing a uniform geometric layout. They are clustered buildings, which are unique in their appearance and layout (Fig. 1(d)). Regular Housing (*reghous*) comprises single family houses with a high proportion of greening between the spaces and is prevalent in the suburbs of a city (Fig. 1(e)).

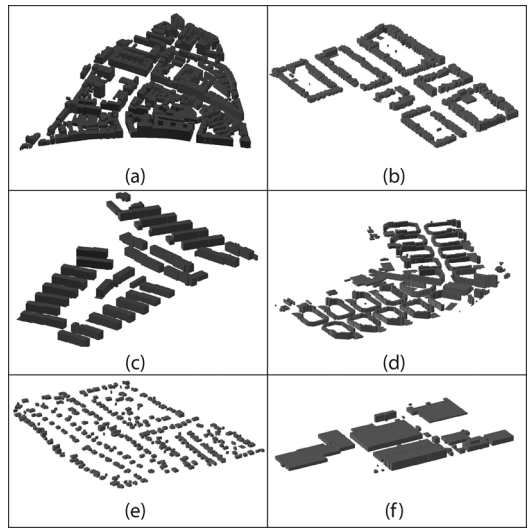

Fig. 1. Illustrations of selected LCZ morphologies in Hamburg: (a) urban core, (b) urban dense, (c) terraced housing, (d) blocks, (e) regular housing, (f) industrial.

While the original LCZ system distinguishes between 'Industrial Processing' (heavy industry) and 'Extensive Lowrise' (light industry, industrial parks and commercial), this differentiation did not seem perfectly suitable for Hamburg, which comprises large harbor areas but little heavy industry outside the harbor region. Therefore, the class *industr* combines both industrial and commercial activities in low-rise buildings. Such large halls are spaced apart and usually appear in clusters (Fig. 1(f)). An additional class *(port)* was introduced to describe the areas associated within the harbor including structures like container-arrays or storage facilities. Modern Core (*modcore*) outlines high rise buildings with a commercial function which in most cases provide the highest buildings of a city, although in Hamburg they are fairly lower than those of common central US business districts. Generally, they are either clustered near the inner city or appear as single buildings within other structures. The classes are complemented by rail tracks (*rail*), urban green (*park*) and *gardens*. The LCZ 'Open Ground' was not applicable, as European morphologies are rather compact avoiding extensive land consumption.

Regarding the agricultural and natural classes, only few were relevant for the area of interest. Fields (*field*) were not further differentiated regarding the plant cover status, because input data with different phenologic conditions was used. *Forest* is a combination of different forest types and trees. Eventually, *water* bodies were added as an additional class.

Representative training areas were digitized for all classes (Fig. 2). For the processing a regular grid with 100 m spacing was chosen considering typical building block ranges and the microclimatic scales discussed above.

The southern part of Hamburg, Germany (53.38 – 53.63°E, 9.75 – 10.38°N) was selected as study area, comprising the Elbe River (from South-East to North-West), the harbor areas (in the center), the city center densely populated areas (north of it), and forested areas in the South and East. Hamburg is situated in the northern German lowlands between the North Sea and the Baltic Sea.

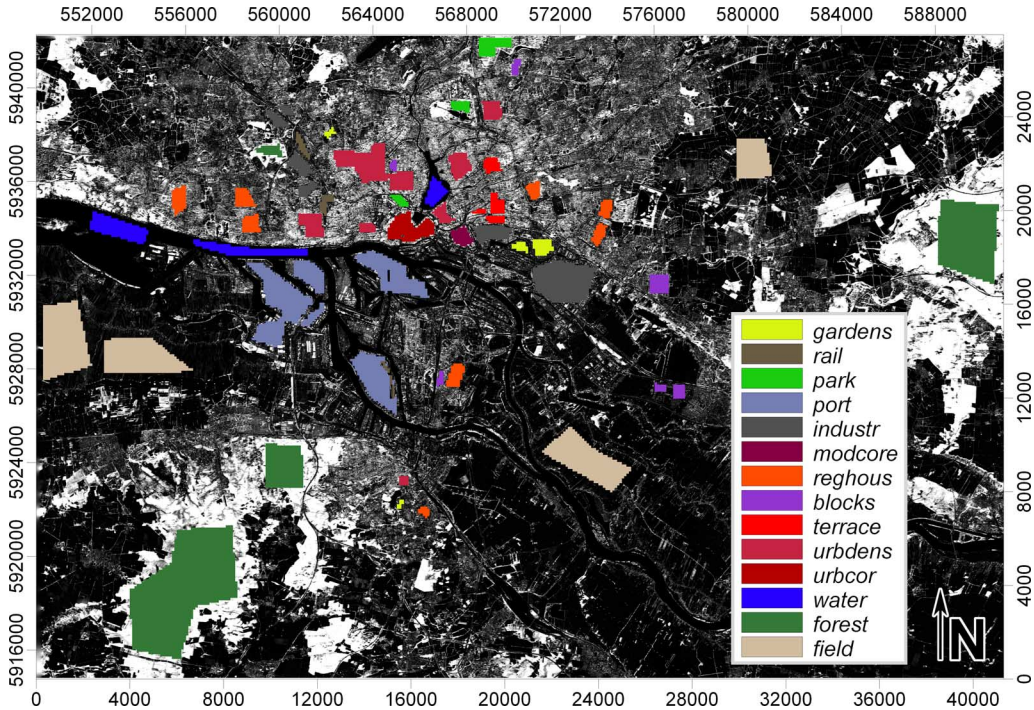

Fig. 2. Study area and training areas for different classes; background IFSAR-NDSM.

TABLE II
FEATURE SETS AND NUMBER OF FEATURES N PER SET

featset	description	N
ndsm	simple height statistics	6
acp	annual cycle parameters: YAST/MAST	2
ms	TM/ETM+ multispectral	231
morph	morpholocigal opening & closing profile	22
fft	fourier transform bandpass filters	190
tir	TM/ETM+ thermal infrared	33
	overall	484

B. Features

Six feature sets were investigated, representing morphology, thermal surface conditions and reflectance in different wavelength bands. All features were derived from data of three different sensors, an airborne Interferometric Synthetic Aperture Radar (IFSAR), the Thematic Mapper (TM) onboard Landsat 5 and the Enhanced Thematic Mapper Plus (ETM+) onboard Landsat 7. All features were projected and resampled to a common 100 m grid using an area weighted mean of the respective grid cells. The derived feature sets are summarized in Table II.

The NDSM was created from the NEXTMap® Digital Surface Model (DSM) and Digital Terrain Model (DTM) products from Intermap Technologies. Both datasets were generated with Intermap's IFSAR technology flown on an aircraft at 8500 m flight height with 45° viewing angle. While the DSM represents the average height of the main scattering elements in a grid cell, for the DTM data product, obstructed areas (buildings and vegetation) are eliminated. Large water bodies are assigned the elevation of the shoreline. The NDSM is the difference between the DSM and the DTM and hence contains solely the obstacles without the topography. In [25] it was shown that the frequency distribution of heights is related to aerodynamic roughness, a property in the LCZ fact sheets. The NDSM was projected to a 3 m UTM32 grid, which is slightly above the specified resolution of the data products. As parameters of the height distribution minimum, maximum, range, mean, variance and standard derivation of the 3 m NDSM were derived for each 100 m grid-cell. For this study ten tiles of the NEXTMap® Products were available.

The multispectral (MS) feature set was derived from 33 cloud-free TM and ETM+ scenes between 1987 and 2010. They were preprocessed with SAGA (www.saga-gis.org) as described in [31]. The multispectral bands 1–5 & 7 ranging from 450–520 nm (visible blue) to 2.09–2.35 μm (medium infrared) [32] were used. Further, the Normalized Differenced Vegetation Index (NDVI) was computed from the bands 3 and 4 resulting in a total of 231 multispectral features. Atmospheric correction was not considered necessary here, since all features were used in trained classifiers and the atmospheric conditions were expected to be fairly homogenous within the area of interest.

The thermal infrared (TIR) data from TM and ETM+ (Band 6, 10.4–12.5 μm) was processed accordingly. Since the calibration to radiance and the derivation of brightness temperatures are at least in good approximation a linear transformation for the given range and all classifiers are trained the digital numbers can be used directly.

The annual cycle parameters (ACP) utilize a simple model of the annual cycle of surface temperatures to derive material specific thermal parameters of the surface [33]. For this study the Yearly Amplitude of Surface Temperature (YAST) and Mean Annual Surface Temperature (MAST) were extracted on the 100 m grid. The surface temperatures were generated from the TM

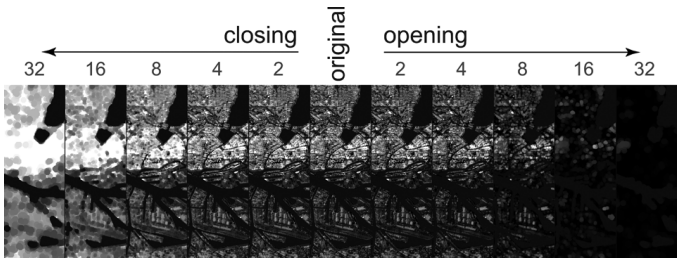

Fig. 3. Morphological profile for a subset of the Hamburg NDSM; closing and openings with different size disk shaped structuring elements.

and ETM+ thermal infrared data using calibration [32] and atmospheric correction [34]. The number of scenes with full-coverage and available reanalysis data was only 22. However, the parameters were used with trained classifiers only and not transferred to other domains, thus full coverage and homogeneity seem more important than the precision of the extracted parameters.

Morphological profiles allow the inclusion of spatial information in a pixel-wise classification approach [35], [11], [36], [12]. Such a profile consists of a series of images transformed with mathematical morphology operators. The basic morphological operators are *erosion* and *dilation*. Both use a structuring element, basically a mask of a region around each pixel. Erosion sets all pixels to the minimum of the surrounding pixels covered by the structuring element whereas dilation sets them to the maximum [37]. The *opening* operator dilates an eroded image with the same structuring element conserving the shape of larger structures whereas small structures completely vanish. Analogously, the *closing* operator performs erosion after dilation. A morphological profile is a series of openings and closings with structuring elements of different size thus eliminating structures (or gaps) of different sizes [35], [10]. The technique was used with high resolution hyperspectral data [35], [11], [36], [12]. However, since it treats the input grayscale matrixes as 'morphologies' it is only consequent to also use it on a NDSM. For this study *opening* and *closing* with disk shaped structuring elements with radii of 2 to 32 pixels were applied to the high resolution NDSM (cf. Fig. 3). As final parameters mean and standard derivation of all pixels in the 100 m grid cell were computed for the full profile.

To include features representing granularity, orientation, and texture of the structures, a windowed multiband signature analysis was chosen. This approach was successfully applied for the semi-automated classification of mixed forests [38]. A Fast Fourier Transform (FFT) was performed for the NDSM within each 100 m grid-cell deriving a 2D spatial spectrum of the contained structures. The data were multiplied with a kernel function in the spatial domain prior Fourier transformation reducing negative effects of the box filter in the frequency domain. The spectrum was subsequently multiplied with a series of bandpass-filters combined with directional filters (cf. Fig. 4). The final spectral signature was a vector containing magnitude and phase of the mean, mean of the real and imaginary part as well as the standard derivation of the magnitude of the spectrum multiplied with each mask. The resulting redundancy was considered unproblematic due to the subsequent feature selection and the large number of filters increased the chance to identify relevant parts of the spectrum.

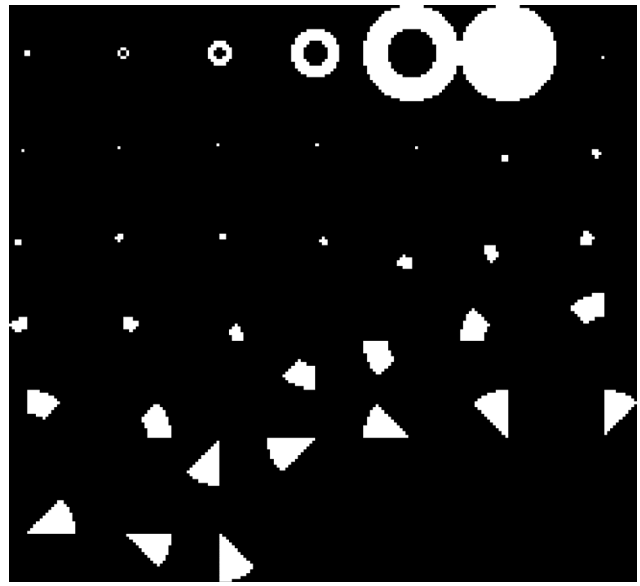

Fig. 4. Bandpass filters applied in the windowed multiband signature analysis.

C. Feature Selection

Different feature selection algorithms such as Discriminant Analysis Feature Extraction (DAFE) [11], Decision Boundary Feature Extraction (DBFE), and Nonparametric Weighted Feature Extraction (NWFE) [11], [12] were successfully applied in urban remote sensing. In this study the Minimum Redundancy Maximal Relevance approach (MRMR), originally developed in bioinformatics for genome classification [39], [40], was tested. The algorithm addressed to the challenge that the individually most relevant features might be highly redundant and therefore classification results may not be substantially improved by additional features. Hence, both the relevance for classification V_I (should be high) and the redundancy with the prior selected feature set W_I (should be low) were combined in a single criterion function in MRMR. Both combined criteria proposed in [39], the Mutual Information Difference (MID) $\max(V_I - W_I)$ and the Mutual Information Quotient (MIQ) $\max(V_I/W_I)$, were tested in this paper. The Mutual Information I is the measure for the similarity between two features and defined as

$$I(x,y) = \sum_{i,j} p(x_i, y_j) \log \frac{p(x_i, y_j)}{p(x_i)p(y_j)} \tag{1}$$

where $p(x,y)$ is the joint probabilistic distribution and $p(x)$ and $p(y)$ are the respective marginal probabilities. In [40] it was shown that the combined criterion MID is recursively (means for any feature set size) more characteristic than the maximal relevance criterion alone and that it is equivalent to the maximal dependency criterion for first-order feature selection.

The authors kindly provide C++ libraries for the computation of Mutual Information and the feature selection for academic use. Since I is defined for discrete data only, all features were linearly divided into 100 classes for feature selection.

TABLE III
CLASSIFIERS

ID	Description	java class (weka.classifiers.)
0R	ZeroR	rules.ZeroR
NB	Naive Bayes	bayes.NaiveBayes
SVM	Support Vector Machine with SMO	functions.SMO
NN	Multilayer Perceptron	functions.MultilayerPerceptron
RF1	Random Forest, 10 trees	trees.RandomForest
RF2	Random Forest, 30 trees, 20 features	
RF3	Random Forest, 50 trees, 30 features	

D. Classifiers

Different classifiers were used in recent studies, including Maximum Likelihood [36], Neural Networks (NN) [9], [36], [11], and Support Vector Machines (SVM) [12]. This study investigated different classifiers. Therefore, two simple classifiers (ZeroR and Naive Bayes) were used as a baseline for three more sophisticated classifiers (Neuronal Network, Support Vector Machine and Random Forest). An overview is given in Table III. The classifiers were all available as java classes in the Weka (Waikato environment for knowledge analysis) data mining package [41], an extensive open source (under GNU General Public License) collection of machine learning algorithms from the University of Waikato.

Zeror (0R): always predicts the most frequent class in the training set (in this case forest, as can be seen from Table I), thus indicating a baseline which should easily be outperformed by any other classifier.

Since the dependency among the different features is usually unknown, the Naive Bayes (NB) classifier makes the simplest assumption of conditional independency. Therefore, the posterior probability of class membership becomes just the product of the marginal probabilities of all features as estimated from the training data. Despite the simplicity of the assumption, it often works quite well in practice [42].

SVM [43] transfer the data into a higher dimensional space with a (non-linear) mapping to increase class separability. Subsequently, an optimal hyperplane is drawn into feature space to separate two classes. For multiclass problems pairwise classification is conducted. Nonlinear decision boundaries can be constructed by the use of kernel functions (i.e., polynomial and Gaussian kernel). Here the default linear kernel was used. The training of the SVM is a very complex quadratic optimization problem, which is reduced to a series of analytically solvable smallest quadratic problems by Platt's Sequential Minimal Optimization Algorithm [44].

A Multilayer Perceptron classifier consists of a feedforward artificial neural network (NN). The NN is a graph representing nodes (neurons) in different connected layers (with the features as input nodes, the classes as output nodes, and *hidden layers* in between). Each node has a weighted non-linear (here sigmoid) activation function, transferring the inputs to the output. The weights of the single nodes determine the output of the entire network and were trained by a backpropagation algorithm. The number of hidden layers was set to the mean of the class number and feature number by default. High dimensional networks construct non-linear decision boundaries of increasing complexity.

Random Forest (RF) by Leo Breiman creates an ensemble of tree-structured classifiers and lets them vote for the most popular class [45]. It is excellent in classification performance and computing efficiency and can handle large data- and feature-sets. For each tree a bootstrap sample is drawn from the full training set. Since a part of the training set is left out for every tree, an unbiased 'out of bag' error estimate can be delivered with the classification. The number of trees grown and the number of features used for each tree can be varied. In this study different configurations were tested. The default classifier RF1 worked with 10 trees, RF2 with 30 trees and 20 features and RF3 with 50 trees and 30 features. The maximum depth of the trees was set to unlimited.

E. Performance Evaluation

For an unbiased evaluation of the classifiers' performance, an independent subset of about 25% of each class was randomly chosen (cf. Table II) and reserved for testing. This sample was not considered during feature selection and classifier training. The accuracy was then evaluated with the testing set only. The following accuracy measures were derived. The *overall accuracy* (OA) is the percentage of correctly classified instances (in this case pixels respective grid cells). The *classification error* is the percentage of incorrectly classified instances. The *confusion matrix* lists the number of correctly and incorrectly classified instances with the reference data in columns and the classifier results in rows. The *producer accuracy* (PA) is the percentage of correctly classified instances of each (reference) class, whereas the *user accuracy* (UA) refers to the percentage of classified instances that indeed belong to the respective class. The *κ-estimate* summarizes different accuracies in a single measure and is defined by

$$\kappa = \frac{P\sum_k x_{kk} - \sum_k x_{k+}x_{+k}}{P^2 - \sum_k x_{k+}x_{+k}} \tag{2}$$

where x_{k+} is the sum over all columns for row k in the confusion matrix and x_{+k} is the sum over all rows for column k [46]. An overview of the full classification and evaluation workflow is given in Fig. 5.

III. RESULTS

The overall accuracies of the classification results from single feature sets are listed in Table IV. For large feature sets, subsets of 10, 20 and 50 features were extracted with MRMR using the MID criterion. As expected, NB outperformed 0R and was itself outperformed by the more sophisticated classifiers (SVM, NN, and RF, further referred to as high-end classifiers). The NB classifier only achieved the best result for the smallest feature set ACP with two features. In general, Multilayer Perceptron and Random Forest classifiers performed best, with some advantages of RF2 for smaller and of RF3 for larger feature sets. The results of the baseline classifier 0R (32.2%) was obviously independent from the feature set.

Regarding the different feature sets, the multispectral (up to 95.1%) and thermal features (up to 96.3%) performed better than the feature sets derived from the IFSAR-NDSM. Within these, the morphological profile performed substantially better

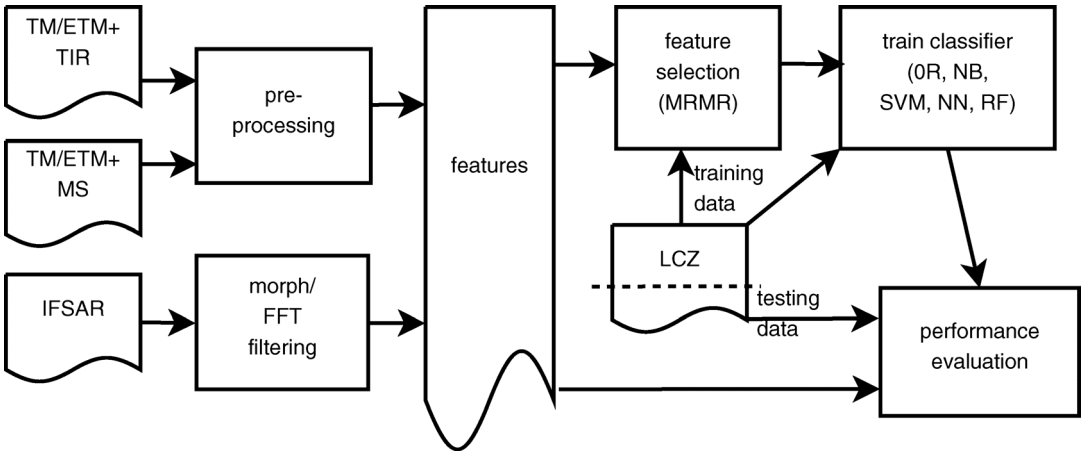

Fig. 5. Workflow of the LCZ classification algorithm and its evaluation.

TABLE IV
LCZ CLASSIFICATION RESULTS FOR SINGLE FEATURE SETS WITH DIFFERENT CLASSIFIERS; FOR LARGE SETS, SUBSETS OF THE TOP 10, 20, AND 50 FEATURES WERE SELECTED BY MRMR WITH THE MID CRITERION. **BOLD** INDICATES BEST RESULT OF EACH FEATURE SET

	CLASSIFIER						
feature set	**0R**	**NB**	**SVM**	**NN**	**RF1**	**RF2**	**RF3**
ndsm	0.322	0.631	0.639	**0.740**	0.716	0.714	0.721
acp	0.322	**0.729**	0.679	0.695	0.710	0.720	0.718
ms(10)	0.322	0.750	0.789	0.846	0.862	**0.872**	0.869
ms(20)	0.322	0.738	0.829	**0.901**	0.898	**0.901**	0.899
ms(50)	0.322	0.730	0.877	**0.926**	0.903	0.917	0.925
ms	0.322	0.735	0.936	**0.951**	0.903	0.925	0.930
morph(10)	0.322	0.723	0.710	0.785	0.805	**0.814**	0.811
morph(20)	0.322	0.677	0.776	0.798	0.801	0.825	**0.830**
morph	0.322	0.672	0.775	0.802	0.799	0.823	**0.832**
fft(10)	0.322	0.648	0.644	**0.717**	0.696	0.703	0.707
fft(20)	0.322	0.625	0.705	0.729	0.726	0.737	**0.745**
fft(50)	0.322	0.606	0.734	0.718	0.720	0.754	**0.757**
fft	0.322	0.595	0.725	0.672	0.692	0.735	**0.748**
tir(10)	0.322	0.720	0.802	0.884	0.892	0.890	**0.894**
tir(20)	0.322	0.701	0.846	**0.934**	0.922	0.921	0.920
tir	0.322	0.683	0.890	**0.963**	0.922	0.938	0.936

(83.2% with RF3) than the simple height statistics (74.0% with NN), whereas the windowed multiband signature only slightly improved the result (75.7% for the top 50 with RF3). The annual cycle parameters performed worse than the other feature sets since it consists of two features only.

Since the feature sets had different sizes, additionally subsets of equivalent sizes (10, 20, and 50 features) were compared with similar results. All high performance classifiers (SVM, NN, and RF) yielded better results with the TIR data, before spectral data, morphological profiles and bandpass features. Only NB always performed best with spectral data before the morphological profiles (for 10 features) and the TIR features (20 features).

Subsequently, it was tested whether the incorporation of multiple feature sets improved the classification. Hence, feature subsets of 10 to 100 features were extracted from the full feature set with MRMR using both, the MID and MIQ criterion. The top 20 selected features are listed in Table V. For both methods, thermal, spectral, and morphological features are represented in the best 5 features and all sets are represented in the best 20 (except FFT for MIQ and strictly NDSM for MID). Hence, as expected the redundancy between different features sets is smaller than within one set. By MID (MIQ) 7 (8) spectral, 5 (4) MORPH, 4 (5) TIR, both (both) ACP, 2 (0) FFT and 0 (1) simple NDSM features were selected within the top 20.

The OA for the different size feature sets with both selection methods are given in Table VI. Generally, the best results were achieved by the Multilayer Perceptron classifier except for a few smaller feature sets, where Random Forest performed slightly better. Accuracies of about 90% were already achieved with 10 selected features. The MID and the MIQ criterion performed almost equivalent with a mean difference of 0.0026 for 10–100 features and all classifiers.

The dependency of the classification error on the size of the feature set (MRMR with MID) is further shown in Fig. 6. The error of NB slightly increased for more then ten features, whereas the error for the other classifiers continuously decreased (SVM and NN) or reached some rather stable lower boundary value (RF). The performance of all RF and NN was almost equal for 10 to 30 features but RF1 only slightly improved with further features and RF2 & RF3 reached their saturation at about 50 features. SVM continuously improved but had larger errors than the other high-end classifiers. It also was the only classifier that had a better result with all 484 features. Hence, NN best exploited larger feature sets, but SVM even improved with a very large feature set.

Tables VII and VIII show the confusion matrices for selected classifiers and feature set sizes (NB with 10 features MID and RF3 with 100 features). For NB there was considerable confusion between the classes *industr* and *port* as well *blocks* and *reghous*. Furher, there was some confusion between *park* and

TABLE V
SELECTED 20 BEST FEATURES BY MRMR (MID & MIQ CRITERIA) AND CORRESPONDING FEATURE SETS; * QUASI EQUVIALENT TO MEAN(NDSM), NO MORPHOLOGICAL FILTERING WAS PERFORMED

mid, discrete_100	featset	miq, discrete_100	featset
LT51960232009184MOR00_B6	tir	LT51960232009184MOR00_B6	tir
orig_mean	morph*	DHMmean	ndsm
close_disk 16mean	morph	LT41960231990076XXX01_NDVI	ms
LT41960231990076XXX01_NDVI	ms	LT51960232009168MOR00_B1	ms
LE71960232000120EDC00_B1	ms	close_disk 32mean	morph
MAST	acp	LE71950232001227EDC00_B6	tir
open_disk 32mean	morph	open_disk 32mean	morph
LT51960232007115MOR00_NDVI	ms	LT51960232007115MOR00_NDVI	ms
LT51950232006185KIS00_B6	tir	LT51950232006185KIS00_B6	tir
std(abs([b2]2[sec]1))	fft	LT41960231990076XXX01_B4	ms
close_disk 32mean	morph	LE71960232000120EDC00_B1	ms
LT51960232009184MOR00_B1	ms	MAST	acp
LE71950232001227EDC00_B6	tir	LT41960231992178XXX02_B6	tir
open_disk 4mean	morph	close_disk 16mean	morph
LT41960231990076XXX01_B4	ms	LE71960232002093EDC00_NDVI	ms
LT41960231992178XXX02_B6	tir	LT51960232009184MOR00_B1	ms
LE71960232002093EDC00_NDVI	ms	YAST	acp
LT51960232009168MOR00_B1	ms	open_disk 8mean	morph
YAST	acp	LT41950231992139XXX02_B6	tir
std(abs([b2]2[sec]2))	fft	LT51960231987188XXX02_B1	ms

TABLE VI
LCZ CLASSIFICATION RESULTS FOR MULTIPLE EO FEATURE SETS SELECTED BY MRMR (MID & MIQ CRITERIA); N: NUMBER OF FEATURES; **BOLD** INDICATES BEST CLASSIFIER FOR FEATURE SET, *ITALICS* BEST FEATURE SET FOR CLASSIFIER

selection		CLASSIFIER					
N	method	NB	SVM	NN	RF1	RF2	RF3
10	MID	*0.831*	0.843	0.885	0.893	0.891	**0.898**
10	MIQ	*0.831*	0.854	**0.909**	0.907	0.906	0.907
20	MID	0.829	0.871	**0.925**	0.923	0.917	0.917
20	MIQ	0.828	0.876	0.920	**0.922**	0.921	0.920
30	MID	0.822	0.881	0.930	0.924	0.925	**0.932**
30	MIQ	0.823	0.888	**0.937**	0.923	0.932	0.925
40	MID	0.822	0.888	0.932	0.921	0.932	**0.935**
40	MIQ	0.822	0.900	**0.949**	0.927	0.939	0.938
50	MID	0.830	0.909	**0.960**	0.924	0.948	0.945
50	MIQ	0.828	0.913	**0.967**	0.933	0.951	0.947
60	MID	0.824	0.916	**0.958**	0.929	0.946	0.951
60	MIQ	0.818	0.919	**0.962**	0.936	0.954	0.950
70	MID	0.822	0.921	**0.967**	0.932	0.947	0.949
70	MIQ	0.815	0.926	**0.964**	0.932	0.949	0.944
80	MID	0.814	0.931	**0.966**	*0.939*	0.948	0.952
80	MIQ	0.816	0.930	**0.963**	0.933	0.953	0.954
90	MID	0.820	0.929	**0.969**	0.929	*0.954*	0.953
90	MIQ	0.819	0.935	**0.969**	0.936	0.949	*0.955*
100	MID	0.821	0.938	**0.969**	0.930	0.948	0.953
100	MIQ	0.818	0.943	***0.974***	0.928	0.947	0.953
all	-	0.801	***0.960***	**0.960**	0.916	0.942	0.946

forest as well as *reghous* and *gardens*. *Modcore* was partly classified as *urbcore*, *terrace* as *urbdens* and *rail* as *port*. This results in lower PA and UA for these classes and consequently a κ-coefficient slightly below the OA. For RF3 there is much less confusion but essentially between the same classes and only *terrace* and *rail* have PAs below 80% whereas all UAs are above 80%.

IV. DISCUSSIONS

In general, we consider classification accuracies above 95% as very good. In other studies, very high accuracies were achieved in classification of urban land cover types and surface materials from hyperspectral data, specifically 98.9% OA for Washington DC, USA, and 93.9% for the center of Paiva, Italy, with a neural network classifier and morphological profiles [11] and 97.5% for Paiva with an ensemble of classifiers [36]. In [12] 98.9% OA were realized for Paiva center and 85.4% for the university campus of Paiva with a SVM. In [9], 78.4% OA were reached for Santa Monica, USA with optical and SAR data and 76.2% with multiband SAR data for Broni, Italy with an NN classifier. Applying VHR optical data and a DSM 90.1% were reached for Cologne and 88.9% for Dresden, Germany [17].

In comparison, the 97.4% achieved in this study with NN and MRMR and the multiple EO Hamburg data are slightly below the best results of other studies. However, a direct comparison with other results must be drawn very carefully, keeping in mind the difference not only in the input data and its resolution but also the variation in class typologies.

Regarding the classification of urban structural types 60% were archived for Munich, Germany, with spatial indicators derived from hyperspectral data with a Minimum Distance approach [47]. For Cologne, Germany, visually convincing classification results were archived with an object-based approach [17], but the quantitative analysis is still pending.

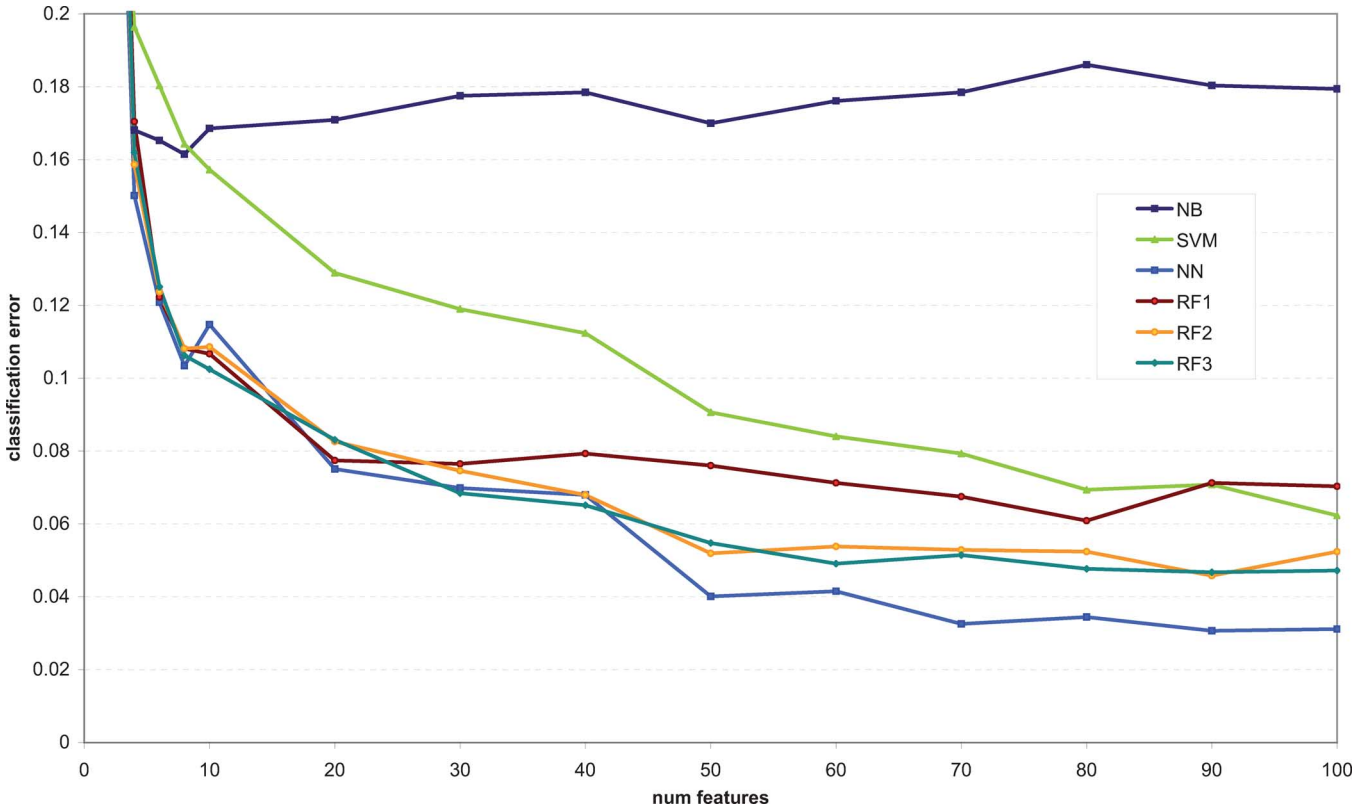

Fig. 6. Classification error for different classifiers and feature set sizes (selected with MRMR, MID).

These results show that the chosen approach has high potential to automatically classify LCZ from multiple source satellite and airborne EO data.

The performance of the classifiers with different feature sets is reasonable. NB delivers moderate results with small features sets but with increasing dimensionality and redundancy the assumption of independence becomes less acceptable. RF1 does not benefit from larger feature sets, since only 10 features are used for each tree. Hence, it was outperformed by RF2 and RF3 for larger feature sets. Regarding the much higher computational effort of NN for large feature sets and the risk of overfitting, RF can still be considered a good alternative.

The MRMR feature selection proofed to be very useful for the classification of urban structures from multiple EO data. The generated small sets of about 10 or 20 features yielded high classification accuracies of 90.9% to 92.5%. Since both criteria performed comparably we recommend the use of MID, which is more robust if further filters are applied according to [40].

Concerning the different feature sets, the well-known and widely used TIR and MS data from ETM showed great potential for the classification of LCZ, which is very pleasant considering their ubiquitary and free availability. The great use of thermal data has been reported before. For instance the identification of surface cover types greatly benefits from the incorporation of thermal data [15], whereas reflectance shows higher separability than multitemporal thermal features for many surface types [16]. However, this also puts emphasis on a combination of both.

We also obtained good results using the IFSAR-NDSM, especially with the morphological profile approach. The annual cycle parameters were outperformed by the other feature sets and it can be acknowledged that the full TIR dataset comprises more information than the ACP. However, taking into consideration that ACP consists of only two features, its performance is still noticeable (the two best MID features reach only 68.3% with NB, 62.0% with RF2 and 67.8% with SVM). The relevance of the features YAST and MAST may be underlined by the fact, that both were voted among the top 20 features with both MRMR approaches.

As expected, the feature sets from multiple EO data performed better for small sets, even if the best result with multiple features were only slightly better than the result of TIR features only. Nevertheless, this surprising performance of the multitemporal TIR data is reasonable when considering that the LCZ system is based on the thermal properties of urban morphologies. Hence, it adds further evidence to the concept even if the canopy layer air temperatures and surfaces temperatures are linked by several complex exchange processes.

Fig. 7 shows a final classification result (NN, 100 features with MIQ, trained on full training set) for the entire domain. The visual investigation reveals a very convincing discrimination between natural, agricultural and urban types and a good discrimination among the urban classes with the City Center (*urbcore*) south of the Alster Lake and *urbdens* and *terrace* west and east of it. Even if single high houses are classified as *blocks*, they are mostly well recognized.

TABLE VII
CONFUSION MATRIX FOR NAIVE BAYES WITH TOP 10 FEATURES SELECTED BY MRMR WITH MID CRITERION

reference / result	blocks	field	forest	gardens	industr	modcore	park	port	rail	reghous	terrace	urbcore	urbdens	water	Σ_{res}	UA
blocks	21	2	0	0	4	0	2	6	0	6	0	0	8	0	49	0.43
field	0	386	2	1	0	0	0	0	0	0	0	0	0	0	389	0.99
forest	0	0	667	0	0	0	1	0	0	0	0	0	0	0	668	1.00
gardens	1	1	0	32	0	0	0	0	0	10	0	0	0	0	44	0.73
industr	1	0	0	0	112	1	0	73	1	0	2	0	5	0	195	0.57
modcore	0	0	0	0	1	8	0	3	0	0	0	6	7	0	25	0.32
park	0	3	13	0	0	0	28	0	0	9	0	0	0	0	53	0.53
port	1	0	0	0	38	0	0	193	9	0	0	0	2	3	246	0.78
rail	0	0	0	0	1	0	0	15	6	0	0	0	0	0	22	0.27
reghous	14	4	0	2	0	0	1	3	0	51	3	0	6	0	84	0.61
terrace	2	0	0	0	2	0	0	2	0	4	12	0	17	0	39	0.31
urbcore	0	0	0	0	1	4	1	1	0	0	0	30	14	0	51	0.59
urbdens	4	0	0	0	4	1	1	9	0	0	14	5	106	0	144	0.74
water	0	0	0	0	0	0	0	0	0	0	0	0	0	109	109	1.00
Σ_{ref}	44	396	682	35	163	14	34	305	16	80	31	41	165	112	**κ**	0.80
PA	0.48	0.97	0.98	0.91	0.69	0.57	0.82	0.63	0.38	0.64	0.39	0.73	0.64	0.97	**OA**	0.83

TABLE VIII
CONFUSION MATRIX FOR RANDOM FOREST (50 TREES, 30 FEATURES) WITH TOP 100 FEATURES SELECTED BY MRMR WITH MIQ CRITERION

reference / result	blocks	field	forest	gardens	industr	modcore	park	port	rail	reghous	terrace	urbcore	urbdens	water	Σ_{res}	UA
blocks	35	0	0	0	1	0	0	0	0	0	0	0	2	0	38	0.92
field	1	395	0	0	0	0	0	0	0	0	0	0	0	0	396	1.00
forest	0	0	680	0	0	0	0	0	0	0	0	0	0	0	680	1.00
gardens	0	0	0	29	0	0	0	0	0	0	0	0	0	0	29	1.00
industr	2	0	0	0	132	1	0	7	1	0	2	1	2	0	148	0.89
modcore	0	0	0	0	1	12	0	0	0	0	0	0	0	0	13	0.92
park	0	0	0	0	0	0	32	0	0	0	0	0	0	0	32	1.00
port	0	0	0	0	24	0	0	293	5	0	1	0	0	2	325	0.90
rail	0	0	0	0	0	0	0	0	10	0	0	0	0	0	10	1.00
reghous	4	1	2	6	0	0	0	0	0	80	2	0	2	0	97	0.82
terrace	0	0	0	0	0	0	0	0	0	0	18	0	1	0	19	0.95
urbcore	0	0	0	0	0	0	0	3	0	0	0	39	4	0	46	0.85
urbdens	2	0	0	0	5	1	2	2	0	0	8	1	154	0	175	0.88
water	0	0	0	0	0	0	0	0	0	0	0	0	0	110	110	1.00
Σ_{ref}	44	396	682	35	163	14	34	305	16	80	31	41	165	112	**κ**	0.94
PA	0.80	1.00	1.00	0.83	0.81	0.86	0.94	0.96	0.63	1.00	0.58	0.95	0.93	0.98	**OA**	0.95

The confusion shown in the matrices above is also quite reasonable. The difference between *industry* and *port* is mostly water access and therefore the given discrimination (see also map) is remarkable. Likewise, the port area contains many rail tracks. Since the *park* class also contains sparse trees, some confusion with *forest* cannot be avoided, as well as between *reghous* and *gardens*. Similarly, since *urbcore*, *terrace* and *urbdens* are not discrete morphological forms but rather typical instances within a continuum, a certain confusion could also be expected. Certainly, the typology can be further improved but in general the results are seen as a confirmation of the adapted LCZ-scheme.

V. CONCLUSIONS AND OUTLOOK

It was shown, that a system of LCZ can be automatically determined from multiple EO data in a trained pixel-based classification approach on a 100 m resolution. Especially, multitemporal Landsat thermal infrared and multispectral data had great potential for an automated LCZ classification, but morphological profiles of the IFSAR-NDSM also were promising. The multiple source feature sets were even better and also showed high classification accuracies with ten or twenty features. Our study demonstrated the suitability of the chosen MRMR feature selection approach for urban remote sensing applications. All high-end classifiers proved useful for the LCZ classification with slight advantages of Random Forest for small, Multilayer Perceptron for large (< 100) and Support Vector Machine for extra large feature sets.

The convincing classification results further provide evidence for the importance of LCZ from an EO point of view which could prospectively serve as interface for urban climatologic purposes. However, the applicability of the classification system adjusted to the particular landscaping of Hamburg needs further investigation on other European and Non-European cities.

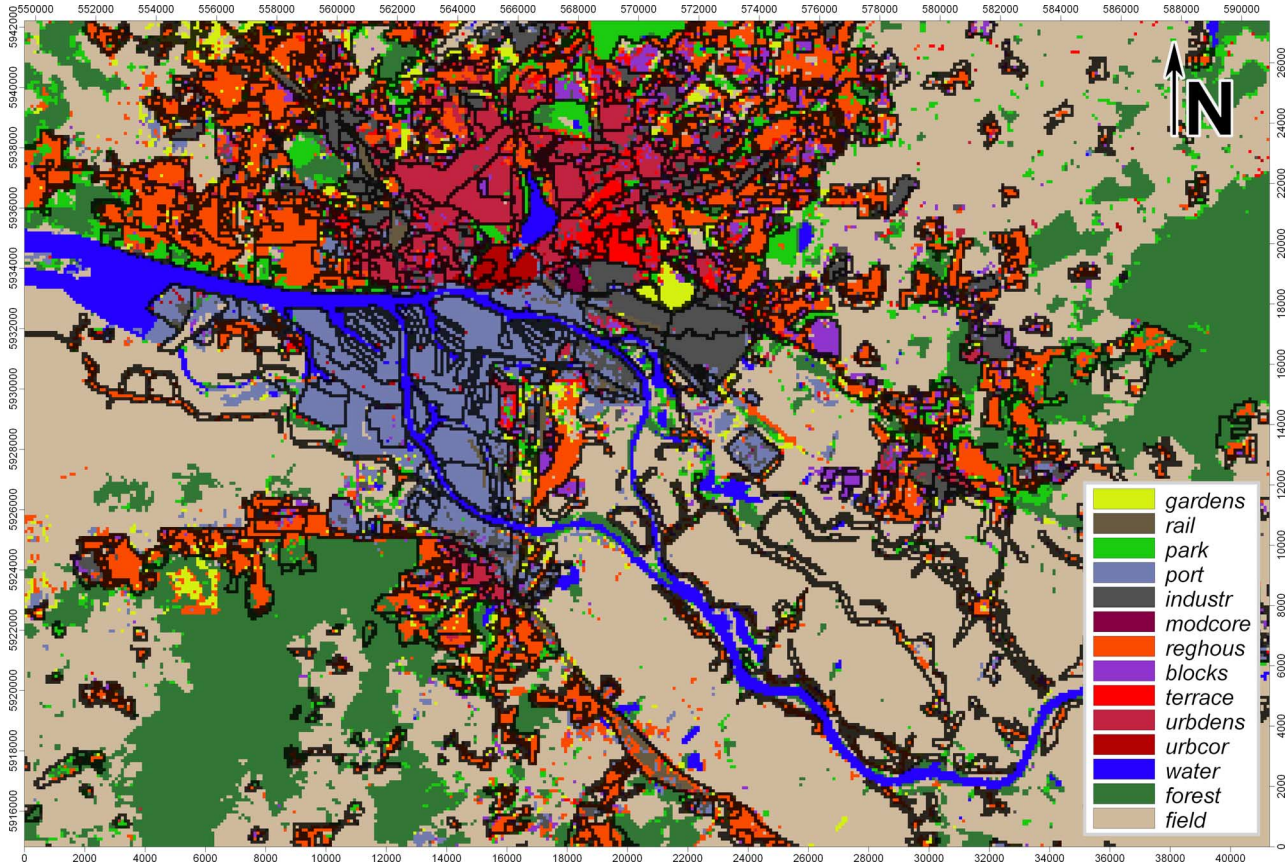

Fig. 7. LCZ classification for the full domain; Multilayer Perceptron classifier with the top 100 features selected by MRMR (MIQ). Mixed classes overlay is from digitized map data.

Regarding the features, other data like SAR intensity or hyperspectral could be included and extended morphological profiles and bandpass filters could be tested. Since the NEXTMap® IFSAR data is not yet available worldwide, other digital elevation products like TanDEM-X should be included in a comparison. The results of the pixel-based approach could be refined by post-classification filters to include more context information.

Further, the pixel-based approach should be compared with the more sophisticated object-oriented approaches to assess, whether their results can be reproduced. Therefore, the problem of mixed pixels needs to be addressed, for instance with a 'spectral' unmixing approach based on endmember selection.

Eventually, the use of a standardized system of local climate zones should be promoted in both urban climatology and urban remote sensing as standard typology of urban morphologies and application interface. Therefore, further investigation of the thermal homogeneity of LCZ in the canopy layer is desirable. For Hamburg a mobile measurement campaign with temperature sensors on public buses is currently conducted to attain spatially and temporally extensive *in situ* data.

ACKNOWLEDGMENT

The authors would like to thank H. Peng and colleagues for the MRMR code, the Machine Learning Group at the University of Waikato for WEKA, and J. Böhner and O. Conrad for SAGA-GIS. The authors also thank NASA and Intermap Technologies for the input data, and N. Bechtel for valuable comments on the manuscript.

REFERENCES

[1] T. R. Oke, "City size and the urban heat island," *Atmospheric Environment*, vol. 7, pp. 769–779, 1973.

[2] T. Yokobori and S. Ohta, "Effect of land cover on air temperatures involved in the development of an intra-urban heat island," *Climate Research*, vol. 39, pp. 61–73, 2009.

[3] M. A. Hart and D. J. Sailor, "Quantifying the influence of land-use and surface characteristics on spatial variability in the urban heat island," *Theoret. Appl. Climatol.*, vol. 95, pp. 397–406, 2009.

[4] M. S. Wong, J. Nichol, and K. H. Kwok, "The urban heat island in Hong Kong: Causative factors and scenario analysis," in *2009 Joint Urban Remote Sensing Event*, Shanghai, 2009.

[5] H. Mayer, A. Matzarakis, and M. Iziomon, "Spatio-temporal variability of moisture conditions within the Urban Canopy Layer," *Theoret. Appl. Climatol.*, vol. 76, no. 3, pp. 165–179, 2003.

[6] Q. Weng, "Thermal infrared remote sensing for urban climate and environmental studies: Methods, applications, and trends," *ISPRS J. Photogramm. Remote Sens.*, vol. 64, no. 4, pp. 335–344, 2009.

[7] C. S. B. Grimmond, "Progress in measuring and observing the urban atmosphere," *Theoret. Appl. Climatol.*, vol. 84, no. 1–3, pp. 3–22, Jun. 2005.

[8] U. Soergel, U. Thoennessen, A. Brenner, and U. Stilla, "High-resolution SAR data: New opportunities and challenges for the analysis of urban areas," *IEEE Proceedings—Radar in Sonar and Navigation*, vol. 153, no. 3, pp. 294–300, Jun. 2006.

[9] P. Gamba and F. Dell'Acqua, "Increased accuracy multiband urban classification using a neuro-fuzzy classifier," *Int. J. Remote Sens.*, vol. 24, pp. 827–834, Jan. 2003.

[10] F. Dell' Acqua, P. Gamba, and A. Ferrari, "Exploiting spectral and spatial information for classifying hyperspectral data in urban areas," in *Proc. IEEE IGARSS'03*, 2003, vol. 1, pp. 464–466.

[11] J. A. Benediktsson, J. A. Palmason, and J. R. Sveinsson, "Classification of hyperspectral data from urban areas based on extended morphological profiles," *IEEE Trans. Geosci. Remote Sens.*, vol. 43, no. 3, pp. 480–491, Mar. 2005.
[12] M. Fauvel, J. A. Benediktsson, J. Chanussot, and J. R. Sveinsson, "Spectral and spatial classification of hyperspectral data using SVMs and morphological profiles," *IEEE Trans. Geosci. Remote Sens.*, vol. 46, no. 11, pp. 3804–3814, Nov. 2008.
[13] W. Heldens, "Use of airborne hyperspectral data and height information to support urban micro climate characterisation," Ph.D. dissertation, University of Würzburg, Würzburg, Germany, 2010.
[14] H. Xie, C. Heipke, P. Lohmann, U. Soergel, V. Tong, and W. Shi, "A new binary encoding algorithm for the simultaneous region-based classification of hyperspectral data and digital surface models," *Photogrammetrie-Fernerkundung-Geoinformation*, vol. 2011, no. 1, pp. 17–33, 2011.
[15] K. Segl, S. Roessner, U. Heiden, and H. Kaufmann, "Fusion of spectral and shape features for identification of urban surface cover types using reflective and thermal hyperspectral data," *ISPRS J. Photogramm. Remote Sens.*, vol. 58, no. 1–2, pp. 99–112, 2003.
[16] R. Frank, *Thematic Classification and Determination of Surface Parameters From Airborne Multitemporal Thermal Imagery*. Berlin, Germany: Logos, 2001.
[17] M. Wurm, H. Taubenbock, A. Roth, and S. Dech, "Urban structuring using multisensoral remote sensing data: By the example of the German cities Cologne and Dresden," in *2009 Joint Urban Remote Sensing Event*, Shanghai, 2009, pp. 1–8.
[18] H. Taubenböck, T. Esch, M. Wurm, A. Roth, and S. Dech, "Object-based feature extraction using high spatial resolution satellite data of urban areas," *J. Spatial Science*, vol. 55, no. 1, p. 117, 2010.
[19] Makarau, G. Palubinskas, and P. Reinartz, "Multi-sensor data fusion for urban area classification," in *2011 Joint Urban Remote Sensing Event (JURSE)*, Munich, Germany, 2011, pp. 21–24.
[20] T. R. Oke, "Towards better scientific communication in urban climate," *Theoret. Appl. Climatol.*, vol. 84, pp. 179–190, Jun. 2005.
[21] I. D. Stewart, "Landscape representation and the urban-rural dichotomy in empirical urban heat island literature 1950–2006," *ACTA Climatologica et Chorologica*, pp. 111–121, 2007.
[22] I. D. Stewart and T. R. Oke, "Newly developed "thermal climate zones" for defining and measuring urban heat island magnitude in the canopy layer," in *Preprints, 8th Symp. Urban Environment*, Phoenix, AZ, Jan. 11–15, 2009.
[23] B. Schaaf *et al.*, "First operational BRDF, albedo nadir reflectance products from MODIS," *Remote Sens. Environ.*, vol. 83, no. 1–2, pp. 135–148, Nov. 2002.
[24] T. Esch *et al.*, "Large-area assessment of impervious surface based on integrated analysis of single-date Landsat-7 images and geospatial vector data," *Remote Sens. Environ.*, vol. 113, no. 8, pp. 1678–1690, 2009.
[25] B. Bechtel *et al.*, "Towards an urban roughness parameterisation using interferometric SAR data taking the Metropolitan Region of Hamburg as an example," *Meteorologische Zeitschrift*, vol. 20, no. 1, pp. 29–37, 2011.
[26] B. Bechtel, "Multisensorale Fernerkundungsdaten zur mikroklimatischen Beschreibung and Klassifikation urbaner Strukturen," *Photogrammetrie-Fernerkundung-Geoinformation*, vol. 2011, no. 5, pp. 325–338, 2011.
[27] R. Ellefsen, "Mapping and measuring buildings in the canopy boundary layer in ten US cities," *Energy and Buildings*, vol. 16, no. 3–4, pp. 1025–1049, 1991.
[28] A. Davenport, S. Grimmond, T. Oke, and J. Wieringa, "The revised Davenport roughness classification for cities and sheltered country," presented at the 3rd AMS Urban Env. Symp., Davis, CA, 2000.
[29] I. D. Stewart, "Classifying urban climate field sites by "local climate zones"," *Urban Climate News*, vol. 34, pp. 8–11, 2009.
[30] I. D. Stewart and T. Oke, "Classifying urban climate field sites by "local climate zones": The case of Nagano, Japan," presented at the 7th Int. Conf. Urban Climate, Yokohama, Japan, 2009.
[31] B. Bechtel and K. J. Schmidt, "Floristic mapping data as a proxy for the mean urban heat island," *Climate Research*, vol. 49, pp. 45–58, 2011.
[32] G. Chander, B. L. Markham, and D. L. Helder, "Summary of current radiometric calibration coefficients of Landsat MSS, TM, ETM+ and EO-1 ALI sensors," *Remote Sens. Environ.*, vol. 113, pp. 893–903, 2009.
[33] B. Bechtel, "Multitemporal Landsat data for urban heat island assessment and classification of local climate zones," in *2011 Joint Urban Remote Sensing Event (JURSE)*, Munich, Germany, 2011, pp. 129–132.
[34] J. A. Barsi, J. R. Schott, F. D. Palluconi, and S. J. Hook, "Validation of a Web-Based atmospheric correction tool for single thermal band instruments," in *Proc. SPIE, Earth Observing Systems VIII*, 2005, vol. 58820, pp. 1–7.
[35] M. Pesaresi and J. A. Benediktsson, "A new approach for the morphological segmentation of high-resolution satellite imagery," *IEEE Trans. Geosci. Remote Sens.*, vol. 39, no. 2, pp. 309–320, 2001.
[36] F. Dell'Acqua, P. Gamba, A. Ferrari, J. A. Palmason, J. A. Benediktsson, and K. Arnason, "Exploiting spectral and spatial information in hyperspectral urban data with high resolution," *IEEE Geosci. Remote Sens. Lett.*, vol. 1, no. 4, pp. 322–326, Oct. 2004.
[37] P. Soille, *Morphologische Bildverarbeitung. Grundlagen, Methoden, Anwendung*. Berlin, Germany: Springer-Verlag, 1998.
[38] C. Körber, D. Möller, and C. Kätsch, "Multi-channel texture classification applied to feature extraction in forestry," in *Proc. 2005 IEEE Int. Conf. Electro Information Technology*, 2005, p. 6.
[39] C. Ding and H. Peng, "Minimum redundancy feature selection from microarray gene expression data," in *Proc. IEEE Int. Computational Systems Bioinformatics Conf.*, Los Alamitos, CA, 2003, p. 523.
[40] H. Peng, F. Long, and C. Ding, "Feature selection based on mutual information: Criteria of max-dependency, max-relevance, and min-redundancy," *IEEE Trans. Pattern Anal. Mach. Intell.*, vol. 27, no. 8, pp. 1226–1238, 2005.
[41] R. R. Bouckaert *et al.*, WEKA Manual for Version 3-7-0, University of Waikato, Hamilton, New Zealand, 2009 [Online]. Available: http://ufpr.dl.sourceforge.net/project/weka/documentation/3.7.x/WekaManual-3-7-0.pdf
[42] R. O. Duda, P. E. Hart, and D. G. Stork, *Pattern Classification*. New York: Wiley, 2001.
[43] C. J. C. Burges, "A tutorial on support vector machines for pattern recognition," *Data Mining and Knowledge Discovery*, vol. 2, no. 2, pp. 121–167, 1998.
[44] J. C. Platt, "Using analytic QP and sparseness to speed training of support vector machines," *Advances in Neural Information Processing Systems*, pp. 557–563, 1999.
[45] L. Breiman, "Random forests," *Machine Learning*, vol. 45, no. 1, pp. 5–32, 2001.
[46] J. A. Richards and V. Jia, *Remote Sensing Digital Image Analysis: An Introduction*. New York: Springer Verlag, 2006.
[47] U. Heiden, W. Heldens, S. Roessner, K. Segl, T. Esch, and A. Mueller, "Urban structure type characterization using hyperspectral remote sensing," *Landscape and Urban Planning*. [Online]. Available: http://www.sciencedirect.com/science/article/pii/S0169204612000175

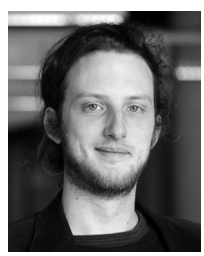

Benjamin Bechtel was born in Heidelberg, Germany. He studied geography, physics, computer science, and urban planning at the University of Hamburg, the Hamburg University of Applied Sciences, and the Hamburg University of Technology. He received the diploma in geography from the University of Hamburg in 2008 and finalized his Ph.D. thesis in 2011.

He is currently working as a research associate in the Cluster of Excellence CliSAP at the KlimaCampus Hamburg. His research interests are in the field of urban remote sensing, in particular the characterization of urban surfaces for applications in urban climatology and the provision and integration of urban canopy parameters for climate models.

Dr. Bechtel is a member of the Hamburg Geographical Society, the European Geosciences Union, and the German Society for Photogrammetry, Remote Sensing and Geoinformation. He acts as a reviewer for several international journals including the IEEE TRANSACTIONS ON GEOSCIENCE AND REMOTE SENSING.

Christian Daneke was born in Darmstadt, Germany. He studied geography at the University of Vienna and majored in cartography and geoinformatics in 2008. His focus was an object oriented classification of nuclear facilities for safeguards applications. Since 2009 he has been wrking toward the Ph.D. degree at the KlimaCampus in Hamburg, Germany, focusing on land use modelling applications for urban climate studies. He is working on classification schemes and the connection between land use modelling and mesoscale climate models.